Armchair graphene nanoribbons: Electronic structure and electric-field modulation

Hassan Raza and Edwin C. Kan
School of Electrical and Computer Engineering, Cornell University, Ithaca, New York 14853, USA
(Received 26 March 2008; revised manuscript received 12 May 2008; published 24 June 2008)

We report electronic structure and electric-field modulation calculations in the width direction for armchair graphene nanoribbons (acGNRs) using a semiempirical extended Hückel theory. Important band-structure parameters are computed, e.g., effectives masses, velocities, and band gaps. For the three types of acGNRs, the p_z orbital tight-binding parameters are extracted if feasible. Furthermore, the effect of electric field in the width direction on acGNRs dispersion is explored. It is shown that for the two types of semiconducting acGNRs, an external electric field can reduce the band gap to a few meV with different quantitative behaviors.

DOI: 10.1103/PhysRevB.77.245434 PACS number(s): 73.22.−f, 73.20.−r, 72.80.Rj

I. INTRODUCTION

Unconstrained graphene is a two-dimensional hexagonal monolayer of carbon atoms. Its unique linear dispersion around the Dirac point and zero band gap[1,2] has generated significant interest.[3,4] Constraining one dimension of graphene results into nanoribbons. The electronic structure of these graphene nanoribbons (GNRs) depends on the width and chirality.[5–12] Two unique GNRs are armchair and zigzag referred to as acGNR and zzGNR in this paper. acGNR has an armchair edge as shown in Fig. 1 and when conceptually rolled to form a nanotube results in a zigzag tube and vice versa. Some experimental techniques have already been used to measure their properties[13,14] and numerous fabrication schemes have been devised.[15–17] Electronic applications of graphene and GNRs are also being sought after.[18–20]

In zzGNRs, the wave functions for conduction and valence bands are localized at the edges.[5,6] In addition, the bands around the Fermi energy have very small dispersion that leads to Stoner magnetism.[5,6] These edge states can be modulated with an external electric field in the width direction, resulting in half metallicity.[21]

In acGNRs, the wave functions associated with bands around Fermi energy are distributed throughout the width of the nanoribbon. However, these bands still can be modulated with an external electric field in the width direction as discussed by Novikov using a continuum model.[22] In addition, due to quantization in one direction, acGNRs have velocities less than those found in unconstrained graphene sheets, and the band structure has a parabolic character around the band edge within a few tens of meV.

In this paper, we focus on acGNRs and study their electronic structure and electric-field modulation in the width direction with a semiempirical extended Hückel theory (EHT). Similar electric-field modulation effects have been studied in carbon nanotubes as well.[23,24] The detailed model has been reported in Ref. 9. EHT parameters are transferable and have been benchmarked with generalized gradient approximation of density-functional theory (DFT) for carbon atoms in graphene structure. EHT is computationally inexpensive and hence appropriate for calculating properties of large systems without compromising accuracy. As an example, up to about 1000-atom electronic structure calculations[25] and up to about 150-atom transport calculations[26] have been reported in silicon based systems with modest computational resources. In this paper, up to about 160-atom calculations are presented. Contributions from five nearest neighbors are included. C-C atomic distance is taken as 1.44 Å, for which EHT parameters have been optimized. We find that incorporating about 3.5% decrease in C-C atomic distance[27] for the edge carbon atoms results in a bandgap increase of about 52 meV for $N=18$ and $W=2.1$ nm and bandgap decrease of about 64 meV for $N=19$ and $W=2.2$ nm acGNR. Small bandgap changes are expected since wave functions for valence and conduction bands are delocalized for acGNR. However, in zzGNR, these wave functions are localized on the edges and any atomic relaxation would have significant effect on the band structure. Since these variations are small in acGNR, we ignore any atomic relaxation in the reported calculations. Atomic visualization is done using GAUSSVIEW.[28]

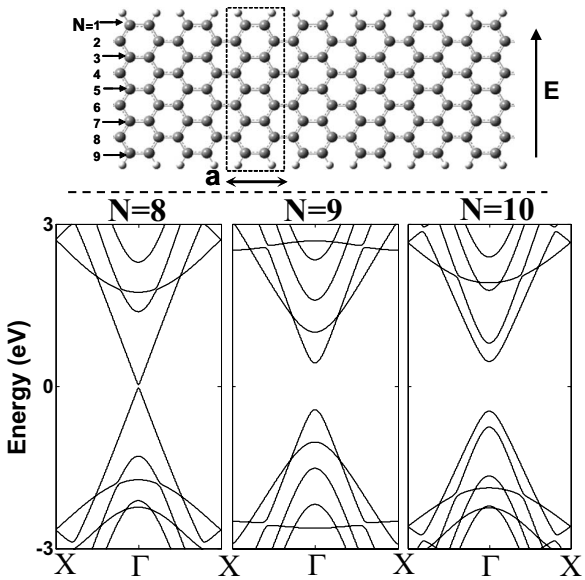

FIG. 1. Electronic structure of acGNRs. The ball and stick model of a graphene nanoribbon with $N=9$ is shown with the unit cell. *E-k* diagrams are shown for three different types of acGNRs using EHT.

II. ELECTRONIC STRUCTURE

On a p_z level of the tight-binding theory, two-thirds of acGNRs are semiconducting with a band gap inversely proportional to their widths and the other has zero band gap depending on the chirality.[5] However, one obtains a different result using the more sophisticated theory,[27] such as EHT and DFT. First, the zero band gap acGNRs also have a small band gap that is inversely proportional to the width. Second, the remaining semiconducting acGNRs only follow an inverse relation within its own category. For convenience, we propose to categorize them into α-, β-, and γ-acGNRs. This classification is similar to the ones used recently in Refs. 27 and 29. α-acGNRs are $N=8,11,14,\ldots$ and have very small band gap. β-acGNRs are $N=9,12,15,\ldots$ and γ-acGNRs are $N=10,13,16,\ldots$ acGNRs have also been classified into three subclasses in context of the orbital diamagnetism.[7]

An electronic structure calculation for each type of acGNR is shown in Fig. 1. As can be seen that $N=8$ α-acGNR has a small band gap and has a nonlinear dispersion around the Γ point. $N=9$ β-acGNR has a large band gap with a parabolic dispersion around the Γ point. Interestingly, $N=10$ γ-acGNR has a slightly larger band gap with larger effective-mass dispersion around the Γ point and smaller velocity in the linear region away from the Γ point as compared to $N=9$ β-acGNR. We extract the band gaps and effective masses within a few tens of meV around the band edges of these three types of acGNRs and plot them in Figs. 2(a) and 2(b), respectively. Figure 2(a) is a computational verification of earlier results[27] on a semiempirical level. We find that incremental change in the band gap of γ-acGNRs with respect to β-acGNRs is smaller in EHT than local-density approximation of density-functional theory.[27] For each type of acGNR, band gaps and effective masses are inversely proportional to the width with a different proportionality constant. The band gap versus width (W) relations are given as

$$E_{\text{gap}} = \begin{cases} 0.04 \text{ eV/W(nm)} & \text{for } \alpha\text{-acGNR} \\ 0.86 \text{ eV/W(nm)} & \text{for } \beta\text{-acGNR} \\ 1.04 \text{ eV/W(nm)} & \text{for } \gamma\text{-acGNR.} \end{cases}$$

We find Fig. 2(b) important because some approaches toward graphene structures involve effective-mass description.[19] Each type of acGNRs follow an inverse relation of effective mass with the width given below,

$$\frac{m}{m_0} = \begin{cases} 0.005/\text{W(nm)} & \text{for } \alpha\text{-acGNR} \\ 0.091/\text{W(nm)} & \text{for } \beta\text{-acGNR} \\ 0.160/\text{W(nm)} & \text{for } \gamma\text{-acGNR,} \end{cases}$$

where m_0 is the free electron mass. It should be noted that using a p_z-orbital tight-binding model, the effective mass follows the same inverse relation versus width for all three types of acGNRs.[19] Furthermore, we determine the p_z-orbital tight-binding parameters that reproduce the band gaps, as shown in Fig. 2(a). These parameters are 2.5 and 2.7 eV for β- and γ-acGNRs, respectively. Since tight-binding parameter for γ-acGNRs is higher, we conclude that the wave functions are hybridized more in this type of acGNR. This physical effect has some implications for electric-field modulation as discussed in Sec. III.

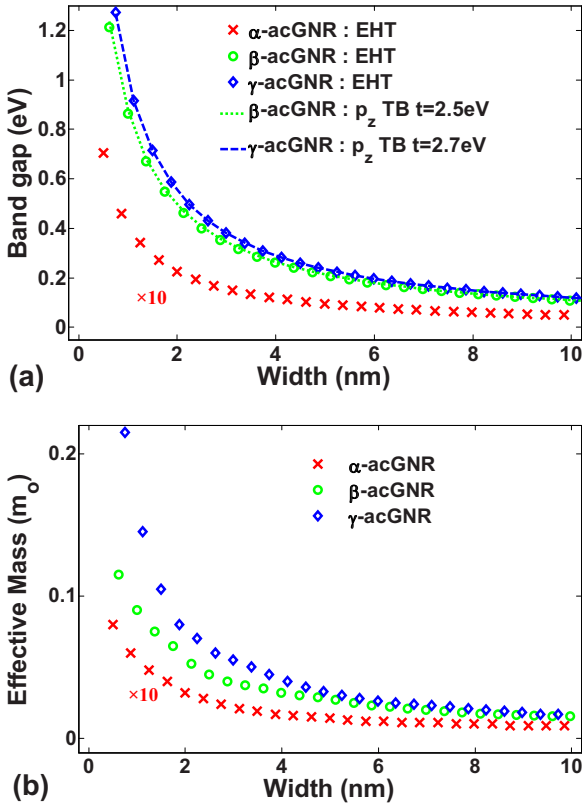

FIG. 2. (Color online) Band gaps and effective masses. (a) Variation of band gap with nanoribbon widths of different types of acGNRs. Using a p_z-orbital tight-binding method, $t=2.5$ eV and $t=2.7$ eV match the band gaps obtained by EHT for β-acGNRs and γ-acGNRs, respectively. (b) Variation of effective mass with nanoribbon widths of different types of acGNRs.

III. ELECTRIC-FIELD MODULATION

Figure 3(a) shows electric-field modulation of the band structure for an $N=10$ γ-acGNR. The effective mass around the Γ point increases with increasing electric field (E) and eventually changes sign, similar to Ref. 22. Furthermore, for $E=0$, the band dispersion in the linear regime away from the Γ point shows velocity very close to the unconstrained graphene velocity ($=8.8\times10^5$ m/s) indicated by red (gray) circles. With increasing E, the velocity in this linear regime away from the Γ point decreases to about 5×10^5 m/s. In addition, the bandwidths of the valence and conduction bands are also decreasing. Moreover, a *Mexican hat* structure is observable that has been seen in acGNR,[22] carbon nanotubes,[24] and graphene bilayers.[9,30–32] These features are in qualitative agreement with the electric-field effects reported in semiconducting acGNRs elsewhere using a continuum model.[22] However, there are some quantitative differences, which we address in this section. We show the extracted effective masses around the Γ point for $N=8$, 9, and 10, which are α-, β-, and γ-acGNRs, respectively, in Fig. 3(b). These effective masses are valid for tenths of k_BT

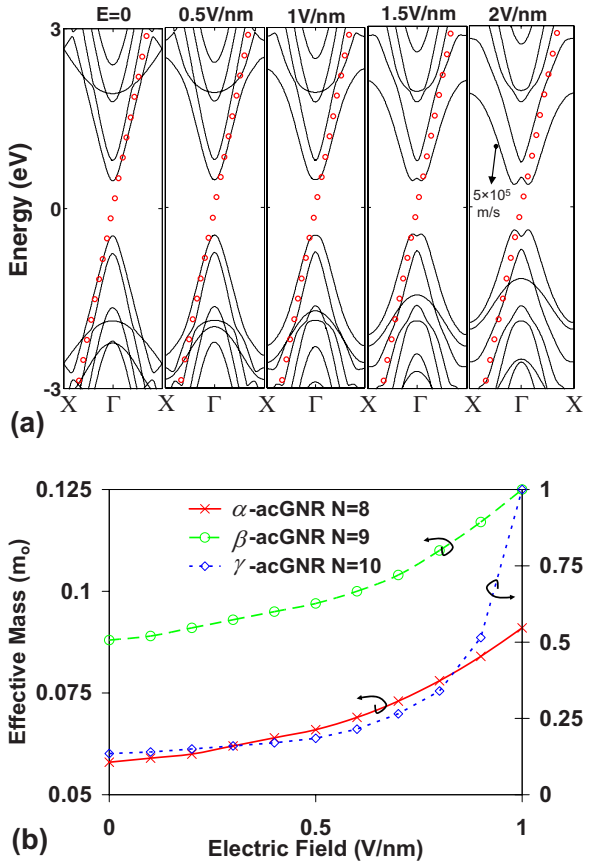

FIG. 3. (Color online) Electric-field modulation of band dispersions. (a) Variation of velocity in the width direction for $N=10$ γ-acGNR. The linear dispersion shown by red (gray) circles represents a value of 8.8×10^5 m/s—velocity around the Dirac point for graphene calculated using EHT. (b) Variation of effective masses. Effective masses are obtained by parabolic fits to the conduction bands within a few k_BT of band edge for β-acGNRs and γ-acGNRs and within a fraction of a k_BT for α-acGNRs.

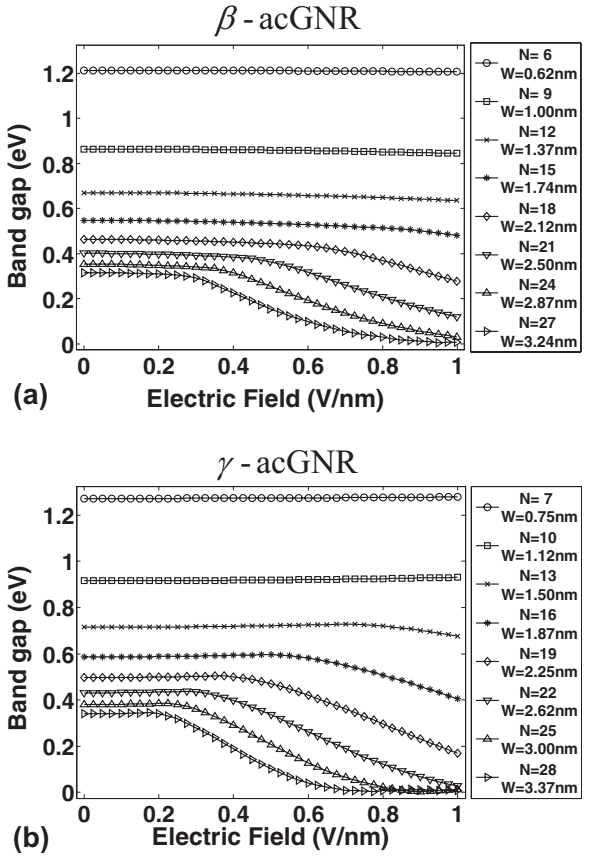

FIG. 4. Band gap modulation. Band gap as a function of width and electric field for (a) β-acGNRs and (b) γ-acGNRs. γ-acGNRs have larger band gap modulation as compared to β-acGNRs.

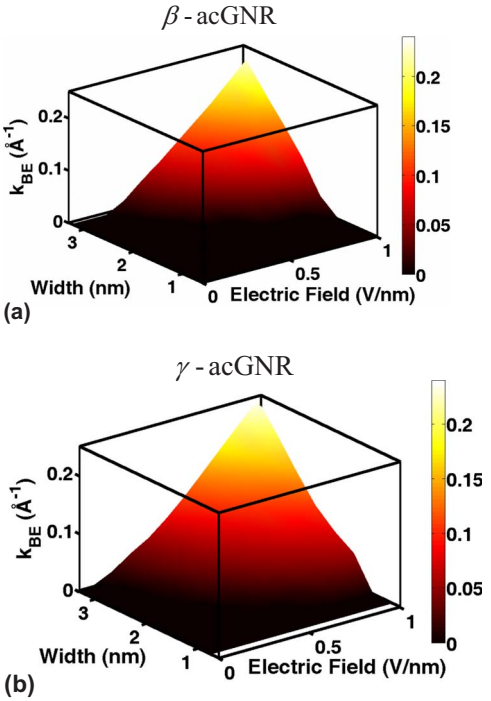

FIG. 5. (Color online) The wave vector corresponding to band edge (k_{BE}) modulation. k_{BE} as a function of width and electric field for (a) β-acGNRs and (b) γ-acGNRs. The value of k at X point is about 0.727 Å^{-1}. γ-acGNRs have larger shift in k_{BE}.

for α-acGNRs and for a few k_BT for β- and γ-acGNRs. After this energy scale, the band dispersions become linear again and remain so for about a few eV when they become nonlinear and hence saturate, as shown in Fig. 3(a). 1 V/nm electric field is within the dielectric breakdown limit of thermal SiO_2, which may result in higher electric field inside graphene due to smaller dielectric constant. Moreover, high-K dielectrics can be used to further enhance the electric field. However, such a high electric field may lead to dielectric reliability issues and is undesirable.

In addition, the band gap is modulated with increasing electric field. A clear feature is the location of wave vector corresponding to the conduction- and/or valence-band minimum and/or maximum. These two perturbations in the band structure are further explored in Figs. 4 and 5, respectively, for β- and γ-acGNRs. In Fig. 4, we show band gap modulation as a function of width and electric field. A threshold behavior is observed, similar to Ref. 22, where band gap starts decreasing appreciably above a threshold electric field E_t. The dimensionless parameter $u_t=eE_t\times W/E_{\text{gap}}$ is reported as 4.5 for both kinds of acGNRs in Ref. 22 using a continuum model. However, we find that this is different for

these two acGNRs and is about 5.6 and 3.9 for β- and γ-acGNRs, respectively. Moreover, for γ-acGNRs, band gap decreases at a faster rate compared to β-acGNRs and thus γ-acGNRs have larger bandgap modulation. This is consistent because wave functions are more hybridized in γ-acGNRs and hence any perturbation affects the band structure more than β-acGNRs.

Additionally, the band gap for β-acGNRs monotonically decrease with electric field. However, the band gap decreases appreciably only after a threshold electric field. This is different from Ref. 22, where below the threshold electric field, band gap is constant and it decreases only after the threshold electric field. Furthermore, for γ-acGNRs, the band gap first increases a little and then decreases—a feature although small but not present in continuum calculations.[22]

With an appropriate electric field applied, one can reduce the band gap of a semiconducting acGNR to a few meV. We find that band gap never becomes zero, whereas using a continuum model,[22] one finds zero band gap. In order to change the band structure, one has to incorporate perturbation on the order of the tight-binding parameter (2.5 eV for β- and 2.7 eV for γ-acGNRs). Therefore, an electric field of 1 V/nm should not be able to induce a significant change in small width acGNRs due to small perturbation as shown in Fig. 4. However, the same electric field can change the electronic structure of a wider acGNRs due to larger potential variation. The physics behind this band gap narrowing is the spectral shift of the conduction- and valence-band states on the two edges. This leads to downward and upward shifts for conduction and valence bands, respectively. Furthermore, in Fig. 5, we show the wavevector shift (k_{BE}) corresponding to conduction-band minimum and/or valence-band maximum. Again, γ-acGNRs have larger shift as compared to β-acGNRs. Overall, this shift can be as much as one third of the wave vector at X point. Unfortunately, we could not find a consistent set of p_z-orbital tight-binding parameters to reproduce Figs. 3–5 simultaneously.

IV. CONCLUSIONS

We have studied band structure and electric-field modulation of acGNRs using EHT. The three types of acGNRs exhibit distinct electronic structure and electric-field modulation properties. We extract important band-structure parameters and a set of p_z-orbital tight-binding parameters benchmarked with extended Hückel theory to reproduce the band gaps. Additionally, electric-field modulation results are compared with a continuum model.[22] We find that qualitative trends are the same; however, there are some quantitative differences between the two models.

ACKNOWLEDGMENTS

The work is supported by National Science Foundation (NSF) and by Nanoelectronics Research Institute (NRI) through Center for Nanoscale Systems (CNS) at Cornell University. We are grateful to Tehseen Raza for GAUSSVIEW (Ref. 28) visualizations and for reviewing the paper. We also thank D. S. Novikov for useful discussions.

[1] P. R. Wallace, Phys. Rev. **71**, 622 (1947).
[2] R. Saito, G. Dresselhaus, and M. S. Dresselhaus, *Physical Properties of Carbon Nanotubes* (Imperial College, London, UK, 1998).
[3] A. K. Geim and K. S. Novoselov, Nat. Mater. **6**, 183 (2007).
[4] A. H. Castro Neto, F. Guinea, N. M. R. Peres, K. S. Novoselov, and A. K. Geim, arXiv:0709.1163, Rev. Mod. Phys. (to be published).
[5] K. Nakada, M. Fujita, G. Dresselhaus, and M. S. Dresselhaus, Phys. Rev. B **54**, 17954 (1996).
[6] M. Fujita, K. Wakabayashi, K. Nakada, and K. Kusakabe, J. Phys. Soc. Jpn. **65**, 1920 (1996).
[7] K. Wakabayashi, M. Fujita, H. Ajiki, and M. Sigrist, Phys. Rev. B **59**, 8271 (1999).
[8] T. Kawai, Y. Miyamoto, O. Sugino, and Y. Koga, Phys. Rev. B **62**, R16349 (2000).
[9] H. Raza and E. C. Kan, arXiv:0801.1125, J. Comput. Electron. (to be published).
[10] V. Barone, O. Hod, and G. E. Scuseria, Nano Lett. **6**, 2748 (2006).
[11] Z. Chen, Y.-M. Lina, M. J. Rooksa, and P. Avouris, Physica E (Amsterdam) **40**, 228 (2007).
[12] L. Brey and H. A. Fertig, Phys. Rev. B **73**, 235411 (2006).
[13] M. Y. Han, B. Ozyilmaz, Y. Zhang, and P. Kim, Phys. Rev. Lett. **98**, 206805 (2007).
[14] T. Enoki, Y. Kobayashi, and K.-I. Fukui, Int. Rev. Phys. Chem. **26**, 609 (2007).
[15] X. Li, X. Wang, L. Zhang, S. Lee, and H. Dai, Science **319**, 1229 (2008).
[16] K. S. Novoselov, A. K. Geim, S. V. Morozov, D. Jiang, Y. Zhang, S. V. Dubonos, I. V. Grigorieva, and A. A. Firsov, Science **306**, 666 (2004).
[17] C. Berger, Z. Song, X. Li, X. Wu, N. Brown, C. Naud, D. Mayou, T. Li, J. Hass, A. N. Marchenkov, E. H. Conrad, P. N. First, and W. A. de Heer, Science **312**, 1191 (2006).
[18] G. Fiori and G. Iannaccone, IEEE Electron Device Lett. **28**, 760 (2007).
[19] G. Liang, N. Neophytou, D. E. Nikonov, and M. S. Lundstrom, IEEE Trans. Electron Devices **54**, 677 (2007).
[20] G. Gu, S. Nie, R. M. Feenstra, R. P. Devaty, W. J. Choyke, W. K. Chan, and M. G. Kane, Appl. Phys. Lett. **90**, 253507 (2007).
[21] Y.-W. Son, M. L. Cohen, and S. G. Louie, Nature (London) **444**, 347 (2006).
[22] D. S. Novikov, Phys. Rev. Lett. **99**, 056802 (2007).
[23] Y. Li, S. V. Rotkin, and U. Ravaioli, Nano Lett. **3**, 183 (2003).
[24] D. S. Novikov and L. S. Levitov, Phys. Rev. Lett. **96**, 036402 (2006).
[25] H. Raza, Phys. Rev. B **76**, 045308 (2007).
[26] H. Raza and Edwin C. Kan, arXiv:0803.1699 (unpublished).
[27] Y.-W. Son, M. L. Cohen, and S. G. Louie, Phys. Rev. Lett. **97**,

216803 (2006).
[28] R. Dennington II, T. Keith, J. Millam, K. Eppinnett, W. L. Hovell, and R. Gilliland, *GaussView, Version 3.0* (Semichem, Shawnee Mission, KS, 2003).
[29] B. Sahu, H. Min, A. H. MacDonald, and S. K. Banerjee, arXiv:0801.1991 (unpublished).
[30] E. McCann, Phys. Rev. B **74**, 161403(R) (2006).
[31] H. Min, B. Sahu, S. K. Banerjee, and A. H. MacDonald, Phys. Rev. B **75**, 155115 (2007).
[32] E. V. Castro, K. S. Novoselov, S. V. Morozov, N. M. R. Peres, J. M. B. Lopes dos Santos, J. Nilsson, F. Guinea, A. K. Geim, and A. H. Castro Neto, Phys. Rev. Lett. **99**, 216802 (2007).